ELSEVIER

Surface Science 490 (2001) 133–143

SURFACE SCIENCE

www.elsevier.com/locate/susc

Adsorption and reaction of gaseous H(D) atoms with D(H) adatoms on Pt(1 1 1) and Sn/Pt(1 1 1) surface alloys

Harald Busse [a], Michael R. Voss [a], Dmitri Jerdev [a], Bruce E. Koel [a,*], Mark T. Paffett [b,*]

[a] *Department of Chemistry, University of Southern California, SSC 606 Los Angeles, CA 90089-0482, USA*

[b] *Los Alamos National Laboratory, Chemical Science and Technology Division, MS J565, Los Alamos, NM 87544, USA*

Received 4 December 2000; accepted for publication 18 May 2001

Abstract

The reaction of gas phase H(D) atoms with adsorbed D(H) atoms on Pt(1 1 1) and two different Sn/Pt(1 1 1) surface alloys was studied by temperature programmed desorption (TPD). The incident H(D) atoms were produced by thermal dissociation in a Pt tube source operated at 1300 K. The alloy surfaces were prepared in situ by vapor deposition of Sn onto a Pt(1 1 1) single crystal to form the (2×2) and $(\sqrt{3} \times \sqrt{3})R30°$-Sn/Pt(1 1 1) surfaces, which have a well-defined structure and composition with relative Sn surface concentrations of 0.25 and 0.33, respectively. A kinetic barrier eliminates dissociative $H_2(D_2)$ chemisorption on both of these surface alloys, but abstraction reactions of incident H(D) atoms with preadsorbed H or D adatoms occur at 110 K on Pt(1 1 1) and both Pt–Sn alloys. This is well below the temperatures for thermal recombination on these surfaces, indicating that the reactions proceed by a direct or pseudo-direct reaction mechanism. Values for the $H \rightarrow D$ abstraction cross-section, σ^R, on Pt(1 1 1) and the (2×2) and $(\sqrt{3} \times \sqrt{3})R30°$-Sn/Pt(1 1 1) surface alloys were determined to be 0.21, 0.93, and 1.7 Å^2, respectively. The corresponding $D \rightarrow H$ abstraction cross-sections for the two alloys were determined to be 0.8, and 1.5 Å^2, respectively. The values of σ^R for both $H \rightarrow D$ and $D \rightarrow H$ reactions increase with Θ_{Sn} and indicate a significant structural sensitivity for H abstraction reactions. There is no significant kinetic isotope effect on either alloy surface, however there is evidence that incident H atoms are slightly more efficient in abstracting adsorbed D atoms than vice versa.

Keywords: Hydrogen atom; Deuterium; Low index single crystal surfaces; Tin; Platinum; Alloys; Thermal desorption; Atom–solid interactions; Surface chemical reaction

1. Introduction

Reactions of gas-phase species with adsorbates occur predominantly via a Langmuir–Hinshelwood (LH) reaction mechanism that involves the adsorption of the gaseous species on the surface prior to reaction. Since the experimental confirmation of an Eley–Rideal (ER) mechanism [1,2], in which the reaction proceeds directly as a result of the impact between an incident reagent and an adsorbate, there has been increased interest in abstraction and addition reactions induced by gas-phase atomic hydrogen. These investigations

* Corresponding authors. Tel.: +1-505-665-9330; fax: +1-505-665-4631.

E-mail address: mtp@lanl.gov (M.T. Paffett).

0039-6028/01/$ - see front matter
PII: S0039-6028(01)01323-1

include hydrogen abstraction [3–9], halogen abstraction [10–12], and hydrogen addition reactions [9,13–18]. Reactions of atomic hydrogen with adsorbed hydrocarbon molecules can be used to synthesize intermediates in hydrocarbon conversion reactions on surfaces and elucidate important elementary reaction steps and thermodynamic properties [19]. Hydrogenation studies of amorphous C:H surfaces by thermal H(D) atoms [20] have provided a microscopic description of primary reaction steps in low-pressure chemical vapor deposition (CVD) of diamond and diamond-like carbon. In addition, Lossev and Küppers [21] have performed adsorption experiments of the isotopes of H on Be(0 0 0 1) as a model study of plasma–wall interactions in fusion devices.

An additional motivation for examining the kinetics of H(D) ER interactions at Pt and Pt–Sn surfaces arises from recent chemical kinetics modeling [22,23] and experimental testing [24,25] of these catalytic materials in the oxidative dehydrogenation of ethane [26,27]. Understanding the roles of H(D) atoms in homogeneous and heterogeneous reaction chemistry at elevated temperatures over Pt and Pt–Sn surfaces has a profound influence on correctly modeling and developing economic viability of this novel process for ethylene production. Incorporation of ER steps (including rate constants and cross-sections), in addition to LH steps and kinetics has yet to be accomplished for this important new process. Ultimately, these steps and associated kinetic parameters may be required for complete and faithful predictive capabilities associated with this emerging technology [26,27].

In cases where dissociative H_2 adsorption is ineffective in UHV because of appreciable activation barriers (e.g., on Al, Be, and Cu) H-atom dosing is often used to generate an adsorbed hydrogen layer. Even in cases where dissociative H_2 adsorption is facile, H atom dosing can be a convenient source of chemisorbed H atoms in reactivity studies on metal surfaces. Recently, for example, the initial sticking coefficient, S_0, of atomic hydrogen (from a W-source at 1800 K) was determined to be $S_0 = 0.9 \pm 0.1$ on Ni(1 1 0) at 150 K [28]. This compares to $S_0 = 0.43 \pm 0.03$ for molecular hydrogen. In addition, our understanding of how thermal H atoms populate subsurface H bonding sites, as on Cu(1 1 0) [29], and Ni(1 1 1) [30], could be advanced from more detailed knowledge of abstraction reactions. As a specific example, it was observed on Ni(1 0 0) that thermal H(D) atoms enter the bulk via a direct process and that abstraction of adsorbed H(D) occurs with a cross-section competitive to transition into subsurface sites [31].

A kinetic barrier to dissociative $H_2(D_2)$ chemisorption exists on Sn/Pt(1 1 1) surface alloys [32–34] that precludes hydrogen uptake under most UHV conditions [35,36]. This barrier height, E_a, was probed by hyperthermal molecular beam experiments [37]. It was determined that a slight increase in E_a exists for the (2×2) Sn/Pt(1 1 1) alloy, compared to that on Pt(1 1 1) where $E_a = 2$ kJ/mol, but that the barrier on the $(\sqrt{3} \times \sqrt{3})R30°$-Sn/Pt(1 1 1) alloy was about 27 kJ/mol at 300 K. The H(D)-surface bond strength was estimated to be 8% lower on the $(\sqrt{3} \times \sqrt{3})R30°$-Sn/Pt(1 1 1) alloy compared to the other two surfaces [35,36], on the basis of subtracting the experimentally derived value of E_a from the H_2 desorption energy (E_d) derived from H_2 TPD data.

The present report describes the kinetics of abstraction reactions of gas-phase atomic hydrogen impinging on adsorbed hydrogen atoms for two isotope combinations, H-on-D and D-on-H. The value of the reaction cross-sections in abstraction reactions on the Pt and Pt–Sn surfaces can help to distinguish direct versus indirect reaction mechanisms [13]. Reaction cross-sections that are on the order of the collision cross-section of the target species generally indicate a direct reaction mechanism (ER) [38,39]. Larger reaction cross-sections indicate accommodation with the surface before reaction by an indirect mechanism (LH) [40,41]. Herein, we determine surface abstraction rates by measuring the H and D surface concentrations via TPD after reaction of a known precoverage of H or D with a defined number of impinging atoms. This avoids the collection of product molecules in a large angular range that is necessary if one was to monitor the direct reaction products "in real time" [3]. Experiments similar to those described herein have been per-

formed in other laboratories on Ni(1 1 0) [28] and Ru(0 0 1) [42,43].

2. Experimental methods

The measurements were performed in a stainless steel ultrahigh vacuum chamber (1×10^{-10} Torr base pressure) equipped with XPS, UPS, AES, HREELS, LEED, and TPD capabilities, as described previously [44]. Electron spectroscopy was performed with a PHI 15-255G double-pass cylindrical mirror analyzer (CMA). TPD experiments were performed with the sample in line-of-sight of the ionizer of a shielded UTI 100C quadrupole mass spectrometer with the shield nozzle located 1 mm from the sample. Typical heating rates were 2 K/s.

The Pt(1 1 1) crystal (Atomergic, 3N purity, 10 mm diameter, $\pm 0.5°$ orientation) was cleaned using 0.9 keV Ar^+ ion sputtering ($I_{sample} = 0.5$ μA, $\alpha_{in} = 45°$) and annealing cycles at 1200 K, with additional oxygen treatments at $p(O_2) = 5 \times 10^{-7}$ Torr for several minutes with the sample at 950 K in order to eliminate residual carbon. The surface order and periodicity was checked with LEED, and the surface cleanliness was evaluated with AES and also with the position of the H_2 desorption peak in TPD, which has been shown to be sensitive to surface cleanliness [45].

The $(\sqrt{3} \times \sqrt{3})R30°$-Sn/Pt(1 1 1) and (2×2)-Sn/Pt(1 1 1) surface alloys were prepared by Sn deposition from a Knudsen source onto the Pt-(1 1 1) crystal at room temperature followed by annealing at 950 K [46]. AES and LEED were used to verify the surface composition and order. For convenience, we refer to the $(\sqrt{3} \times \sqrt{3})R30°$-Sn/Pt(1 1 1) and (2×2)-Sn/Pt(1 1 1) surface alloys as the $\sqrt{3}$ and (2×2) alloys.

Surface coverages θ are given in monolayers (ML), where 1 ML corresponds to the Pt surface atom density of Pt(1 1 1), i.e., $n_{Pt} = 1.505 \times 10^{15}$ atoms/cm^2. Hydrogen adlayer coverages were determined by using TPD. The conversion factors between TPD areas and $\theta_{H(D)}$ were calibrated by using TPD curves obtained following saturation exposures of H_2 and D_2 using a micro-capillary array directed-beam doser on clean Pt(1 1 1) at 190 K. We assume $\theta_{max} = 0.9 \pm 0.1$ [47,48] for both adsorbed H and D on Pt(1 1 1) when produced from molecular adsorption.

H atoms were produced in a resistively heated, U-shaped Pt-tube, similar to a design described by Engel and Rieder [49]. The hydrogen gas (Matheson H_2, 99.99+% purity; Cambridge Isotope Labs D_2, 99.7% purity) was introduced into the Pt dissociation tube via a Granville-Phillips leak-valve after passing through a liquid-nitrogen cooled trap. The temperature of the Pt-tube source was monitored by an optical pyrometer (Omega OS3708) and was highly reproducible (± 2 K) using a regulated 20 V, 20 A power supply (Hewlett-Packard 6264B). Since the single-crystal sample was also Pt, we were able to verify the emissivity calibration of the pyrometer by comparing the temperature of our Pt(1 1 1) crystal measured with the pyrometer with the independent reading of our chromel–alumel thermocouple attached to the crystal. The deviation of the source temperatures measured using the pyrometer (with the emissivity set to the reported value of 0.30 for Pt [50]) from the Pt(1 1 1) sample temperature measured by the thermocouple was determined to be $\leqslant \pm 5$ K for crystal temperatures slightly lower than our actual source operating temperatures. The internal surfaces of the Pt pyrolysis tube were cleaned via oxygen treatment at elevated temperatures with the oxygen entering directly through the source-gas line at a maximum chamber-background pressure of 1×10^{-7} Torr O_2. Subsequent heating in vacuum and operation of the source using a hydrogen-gas flow purged the tube of residual oxygen.

The operating temperature of the doser was optimized at 1300 K. Fig. 1 shows the influence of doser temperature on θ_D after a fixed D exposure on the $\sqrt{3}$ alloy at 185 K. D-atom exposures were performed using a source-to-sample distance of 8.5 mm and monitored by recording the pressure rise in the background gas of the UHV chamber. We report D-atom exposures using this value for convenient reference purposes. Separate measurements described below established the absolute D-atom flux. At source temperatures of 1150–1350 K, for exposures of 0.03 L (60 s at 5×10^{-10} Torr), the experimental data was described well by using

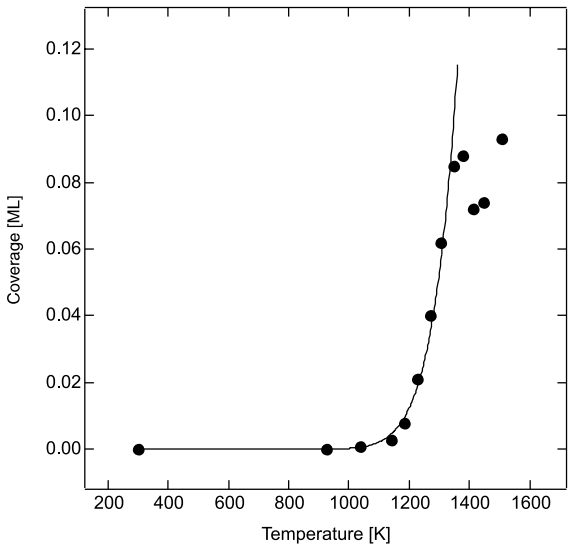

Fig. 1. Measured D uptake on the $\sqrt{3}$ alloy at 185 K as a function of source temperature. The exposure was 0.03 L (60 s at 5×10^{-10} Torr background pressure, mostly D_2). The solid curve was calculated assuming an Arrhenius-type behavior with an activation energy for dissociation of 52 kcal/mol.

an Arrhenius expression with $E_a = 52$ kcal/mol. This value is consistent with the gas-phase bond dissociation energy of D_2, D(D–D) = 104 kcal/mol [51] and implies that no substantial, additional kinetic barrier exists beyond that for bond dissociation. Source operation at temperatures above 1350 K produced irreproducible adsorbed D coverages. These changes are attributed to Pt (or PtH_x) evaporation from the source at these higher temperatures. AES measurements on the Pt–Sn alloys subsequent to D atom dosing with the source operating above 1350 K showed decreases in the Sn/Pt AES ratio consistent with this explanation. In addition, the sharpness of the LEED pattern was affected by these dosing conditions (however, the original state of the surface could be regenerated after a brief annealing of the surface at temperatures around 950 K). Pt evaporation from the doser is expected because Pt has a vapor pressure at 1400 K of $\sim 8 \times 10^{-11}$ Torr [52].

The atomic H(D) flux at a fixed sample–source distance was derived from the initial slope of TPD uptake curves on Pt(1 1 1) at 110 K, assuming an initial sticking coefficient for H(D) atoms of unity and applying an isosteric correction for molecular dissociative adsorption which occurs for Pt(1 1 1) during simultaneous (and unavoidable) $H_2(D_2)$ dosing from the H(D) atom doser. At a source temperature of 1300 K and background chamber pressure of 1×10^{-8} Torr, we determined the flux of the H(D) atom source to be 9.1×10^{13} H atoms/cm^2 s and 5.3×10^{13} D atoms/cm^2 s. This represents a lower limit of the H(D) flux because a value of $S_D < 1$ on Pt(1 1 1) would necessitate higher values. For convenience, the H(D) atom exposures are reported simply as timed exposures in seconds at a given background chamber pressure. The relative ion gauge sensitivity factors for H_2 and D_2 were assumed to be equal according to investigations by Winkler [53] and Jousten and Röhl [54], and the QMS sensitivities for H_2, HD, and D_2 were corrected by factors of 1.0:0.99:0.97 respectively in calculating the TPD areas.

3. Results

Fig. 2 shows the evolution in surface coverage of adsorbed H(D) atoms as the number of incident D(H) atoms on Pt(1 1 1) at 100 K increases. The initial coverages were 0.8 ML, near the saturation coverage achieved by dissociative molecular adsorption on Pt(1 1 1). In the top half of Fig. 2, increasing the H-atom exposure decreases θ_D via desorbing HD molecules. The vacated adsorption sites are available for incoming H atoms, and there is a concomitant increase in θ_H. The solid curves shown to fit the data come from a kinetic analysis of these reactions that will be discussed later and used to determine adsorption and reaction cross-sections. As shown in the figure, the total adsorbate coverage is nearly constant throughout this experiment. In the bottom half of Fig. 2, data obtained for exposures of D atoms on an H-precovered Pt(1 1 1) surface are also shown. This set of curves is shown for completeness but was not used to determine the model parameters described later. This is because a fluctuation in mass spectrometer sensitivity led to an apparent saturation coverage higher than we have previously reported [35].

Fig. 3 shows the analogous plots on the (2×2) alloy. In Fig. 3a, the amount of preadsorbed D

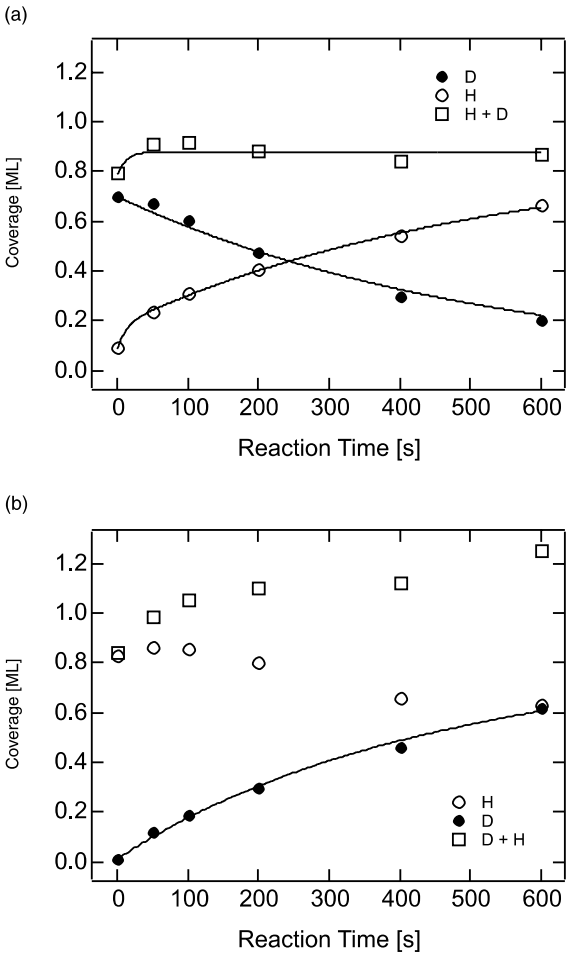

Fig. 2. (a) Reaction of incoming gas-phase D atoms with preadsorbed H atoms on Pt(1 1 1) at 100 K. (b) Reaction of incoming gas phase H atoms with preadsorbed D atoms on Pt(1 1 1) at 100 K.

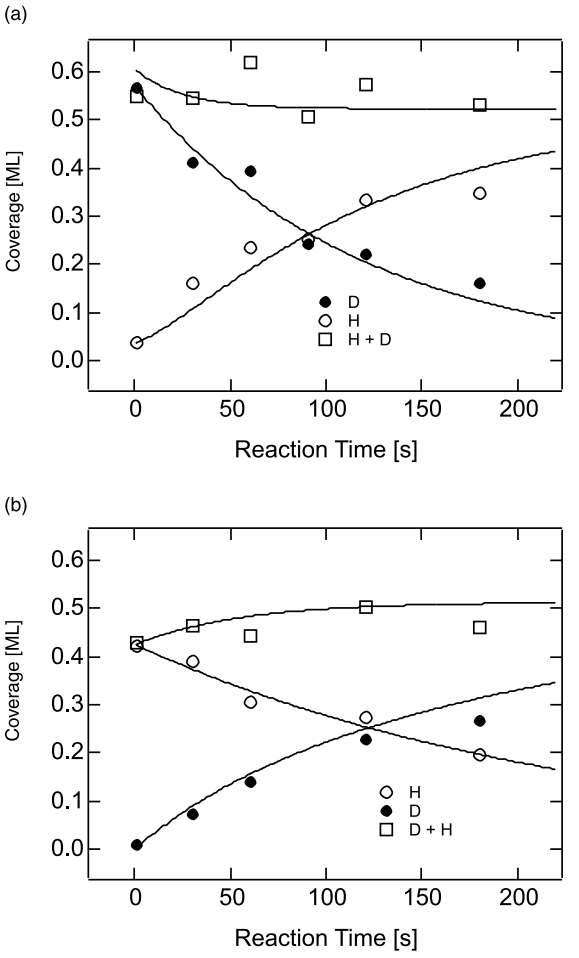

Fig. 3. (a) Reaction of incoming gas phase D atoms with preadsorbed H atoms on the (2 × 2) alloy at 110 K. (b) Reaction of incoming gas phase H atoms with preadsorbed D atoms on the (2 × 2) alloy at 110 K.

was close to the saturation coverage of 0.67 ML on the (2 × 2) alloy, but in Fig. 3b, the initial value of θ_H was slightly lower. The abstraction reaction proceeded to at least 2/3 completion after a 175 s reaction time in both instances, directly indicating higher abstraction rates on the (2 × 2) alloy than on Pt(1 1 1).

Fig. 4 shows the reaction kinetics for the abstraction by H(D) of adsorbed D(H) atoms on the $\sqrt{3}$ alloy. The initial coverage in Fig. 4a was the saturation coverage of 0.51 ML on the $\sqrt{3}$ alloy, but that in Fig. 4b was slightly lower. The rate of abstraction of surface D by incident H atoms was sufficient in this case for the reaction to be run almost to completion, attaining a final equilibrium coverage of the preadsorbed H near zero after 300 s.

4. Discussion

4.1. Kinetic model for abstraction reactions

A simple kinetic model to describe these reactions has been proposed by Jachimowski and

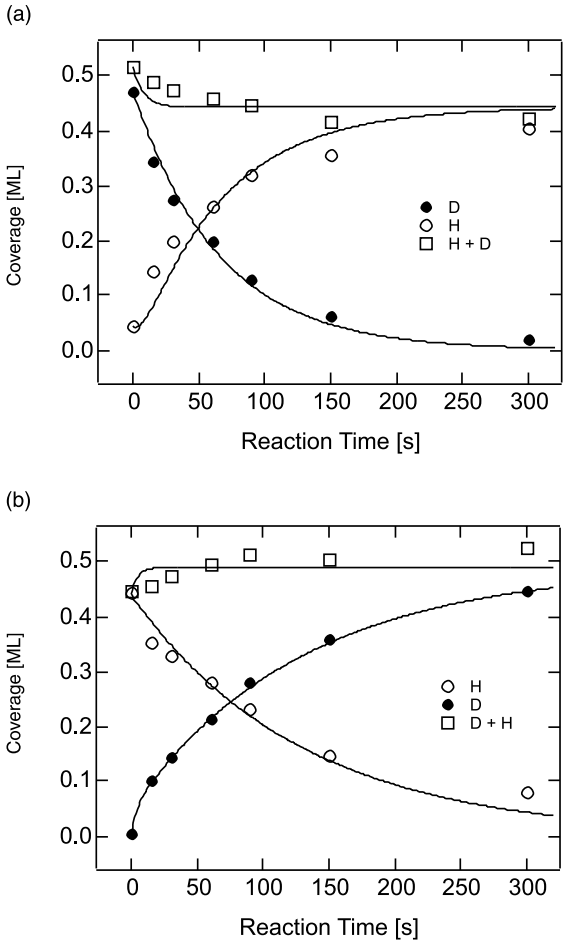

Fig. 4. (a) Reaction of incoming gas phase D atoms with preadsorbed H atoms on the $\sqrt{3}$ alloy at 110 K. (b) Reaction of incoming gas phase H atoms with preadsorbed D atoms on the $\sqrt{3}$ alloy at 110 K.

Weinberg [42]. Assuming first order kinetics, the rate equation for D abstraction by H atoms (H → D) is

$$\frac{d\theta_D(t)}{dt} = -F_H\sigma^R_{(H\to D)}\theta_D(t), \tag{1}$$

where $\theta_D(t)$ is the time-dependent D coverage, F_H is the incoming hydrogen flux, and σ^R is the reaction cross-section for the H → D reaction. This differential equation has the solution

$$\theta_D(t) = \theta_D(t_0)\exp(-F_H\sigma^R_{(H\to D)}t) \tag{2}$$

and describes the decrease in preadsorbed D coverage caused by incident H atoms.

In order to describe the increase in H coverage, $\theta_H(t)$, that occurs during this reaction, we need to include both an adsorption and abstraction term. If both of these reactions are assumed to be first order [42], then one obtains a rate

$$\frac{d\theta_H(t)}{dt} = F_H\sigma^A[\theta_{max} - \theta_D(t) - \theta_H(t)] - F_H\sigma^R_{(H\to H)}\theta_H(t), \tag{3}$$

where, the H adsorption cross-section is σ^A, $\theta_D(t)$ is given by Eq. (2), and the maximum number of available adsorption sites is θ_{max}. This later value was assumed to be independent of the particular isotope, i.e. $\theta_{max(H)} = \theta_{max(D)} \equiv \theta_{max}$. It is simplest to assume (and often done) that the reaction cross-section for the H-on-H abstraction, $\sigma^R_{H\to H}$, and the reaction cross-section for the H-on-D abstraction, $\sigma^R_{H\to D}$, in Eq. (3) are equal and then expressed simply as σ^R [42]. In this case, the general solution to Eq. (3) is

$$\theta_H(t) = (\theta_H(t_0) - s\theta_{max} + \theta_D(t_0)) \times \exp(-F_H[\sigma^A + \sigma^R]t) + s\theta_{max} - f\theta_D(t), \tag{4}$$

where

$$s = \sigma^A_H/(\sigma^R_{H\to H} + \sigma^A_H),$$

$$f = \sigma^A_H/(\sigma^R_{H\to H} - \sigma^A_{H\to D} + \sigma^A_H),$$

and $\theta_D(t)$ is given by Eq. (2).

4.2. Application of kinetic model to the data

Determination of the σ^R values involved fitting Eq. (2) to the decrease in coverage of the preadsorbed species using the data shown in Figs. 2–4. Non-linear least squares fitting was done by utilizing Microsoft Excel®. For the case of H → D, $\sigma^R_{(H\to D)}$ was determined by using the measured values of $\theta_D(t_0)$ and F_H. The incident beam intensity was determined by an independent calibra-

Table 1
Summary of the derived cross-sections (Å^2) for reactions of incident gas-phase H(D) atoms on Pt(1 1 1) and two Pt–Sn surface alloys precovered by adsorbed D(H) adatoms

Reaction	σ (Å^2)	Pt(1 1 1)	(2 × 2) alloy	$\sqrt{3}$ alloy
H → D	σ^R	0.21 ± 0.02	0.93 ± 0.09	1.7 ± 0.16
	σ^A_H	8 ± 3	3 ± 1	11 ± 4
	σ^R/σ^A_H	0.024 ± 0.009	0.28 ± 0.1	0.15 ± 0.06
D → H	σ^R		0.8 ± 0.1	1.5 ± 0.2
	σ^A_D		2.6 ± 0.5	35 ± 10
	σ^R/σ^A_D		0.30 ± 0.07	0.04 ± 0.01

tion to be $F_H = 9.1 \times 10^{13}$ H atoms/cm^2 s ($F_D = 5.3 \times 10^{13}$ D atoms/cm^2 s). Values for σ^R are given in Table 1. For the H → D reaction, σ^R increased from 0.21 Å^2 on Pt(1 1 1) to 0.93 Å^2 on the (2 × 2) alloy and 1.7 Å^2 on the $\sqrt{3}$ alloy. The same trend was observed for the D → H reaction, with σ^R increasing from 0.8 Å^2 on the (2 × 2) alloy to 1.5 Å^2 on the $\sqrt{3}$ alloy.

Determination of the σ^A values involved fitting Eq. (4) to the increase in coverage of the incident species using the data shown in Figs. 2–4 and the σ^R values determined as discussed above. Values for σ^A and σ^R/σ^A are also summarized in Table 1. For the H → D reaction, σ^A decreased from 8 Å^2 on Pt(1 1 1) to 3 Å^2 on the (2 × 2) alloy, and then increased to 11 Å^2 on the $\sqrt{3}$ alloy. A similar trend was observed for the D → H reaction, with σ^A increasing from 2.6 Å^2 on the (2 × 2) alloy to 35 Å^2 on the $\sqrt{3}$ alloy. We also show the solutions for $\theta_{D(H)}(t)$ from Eqs. (2) and (4), using these values for the cross-sections from Table 1, as the solid curves in Figs. 2–4. These curves describe the data reasonably well, affirming the validity of this simple model to describe these processes.

The quality of the fit of these curves to the data also indicates the uncertainty in determining the cross-section values. The error bars reported in Table 1 were obtained by varying σ^A or σ^R values such that this change resulted in a 50% increase in the sum-of-squares characterizing deviations between the experimental values and those predicted by the model. It was noted that obvious visual deviations between the model curves and the data occur at this subjective value. We conclude that the σ^R values are determined with a precision of ~10% while those values for σ^A have a precision of ~30%.

4.3. Abstraction reaction mechanisms

The abstraction of adsorbed D(H) by incident, gas-phase H(D) atoms to produce gas phase HD was observed in our experiments well below the temperatures required to thermally desorb H_2, D_2, and HD from recombination of H(D) atoms on Pt(1 1 1) and the Pt–Sn surface alloys [35]. Additionally, the measured abstraction cross-sections are smaller than the unit-cell size of the substrate (6.65 Å^2 for Pt(1 1 1)). These two characteristics have often been cited as evidence for an ER mechanism [55]. It is now generally understood that there are two other important processes, in addition to a purely ER mechanism. Collision-induced recombinative desorption is one other possible mechanism for these abstraction reactions [56]. In this case, the kinetic energy of an impinging atom supplies the energy necessary for a non-thermal recombination of two adsorbed atoms and molecular desorption. Also, "hot atom" (Harris–Kasemo) reactions may be important processes, where an incoming "hot atom" may lose some energy to the surface (but not enough to chemisorb) and diffuse along the surface and react with an adsorbed species [57].

Our experiments do not directly distinguish between these different, direct reaction mechanisms. Because our coverage measurements are made post-reaction, we measure an overall rate and derive overall reaction cross-sections that include both direct and quasi-direct reaction pathways. However, these separate pathways have been resolved in studies of H/D reactions on Cu(1 1 1) by time of flight mass spectroscopy and product angular distribution measurements [58]. Using the energy distributions of product molecules, Rettner

and Auerbach [59–62] found a variable (translational and vibrational) energy accommodation of "hot" precursor atoms on the surface. Their results show that one can have contributions from both processes simultaneously and there is a gradual transition from an ER to a hot-atom or LH mechanism, requiring corrections to kinetic models to account for precursors such as that proposed by Kisliuk [63].

On Pt(1 1 1), there is direct evidence for the collision-induced desorption mechanism. Wehner and Küppers observed D_2 as a direct H → D reaction product [64] and H_2 as a D → H direct reaction product [65]. We did not monitor for this reaction channel directly, and this pathway would contribute to the measured abstraction cross-sections that we report. Their H-atom source was operated at a much higher temperature (1800–1950 K) than we used in this study (1300 K), but one would expect similar hot-atom reactions in each of these experiments (because of the dominant contribution to the incident atom kinetic energy in each case by the acceleration potential at the surface due to polarization interactions of ~2.5 eV). Thus, it is difficult to explain why they found σ^R values on Pt(1 1 1) (1.25–1.6 Å^2) that are higher than reported here (0.21 Å^2). However, contributions to the measured cross-sections from excited H_2^* reactions should be much greater for experiments carried out with higher doser temperatures, and perhaps this can account for these differences. Or, there is a decreasing contribution due to "hot-atom" reactions at lower doser temperatures where purely ER reactions predominate. Such a trend was also observed by Weinberg and coworkers [66] in H–D atom reaction cross-sections as a function of doser temperature on Ru(0 0 1). Values of σ^R decreased from 1.3–1.4 Å^2 using a high-temperature (1800 K) tungsten filament [42] to 0.47–0.89 Å^2 using a low-temperature microwave discharge source [66].

4.4. Reaction trends on Pt–Sn alloys

It is clear from Table 1 that both $\sigma^R_{D\to H}$ and $\sigma^R_{H\to D}$ increase, i.e., that the abstraction reaction proceeds with a higher probability, with the concentration of Sn present in the surface alloy, from $\Theta_{Sn} = 0$ on Pt(1 1 1) to $\Theta_{Sn} = 0.25$ in the (2×2) alloy and $\Theta_{Sn} = 0.33$ in the $\sqrt{3}$ alloy. In explaining these differences, it is important to remember that these surfaces have quite different structures and chemistry that is not interpreted simply by Θ_{Sn}. Tin atoms in these two alloys occupy Pt lattice positions in the surface layer with Sn buckled out of the surface plane by 0.2 Å. An additional structural difference is noted in that the (2×2) alloy has pure-Pt 3-fold sites, but no two adjacent pure-Pt 3-fold sites as found on Pt(1 1 1), and that the $\sqrt{3}$ alloy has no pure-Pt 3-fold sites at all. These structural differences and the small electronic modification at Pt sites due to alloying results in an energetic barrier to $H_2(D_2)$ dissociation on both alloys and in addition alters the Pt–H(D) bond dissociation energy D(Pt–H(D)). We have previously estimated values for D(Pt–D) on Pt(1 1 1) and the Pt–Sn surface alloys [35], and these results are shown in Fig. 5a. The Pt–D bond strength on Pt(1 1 1) and the (2×2) alloy is nearly the same but decreases by about 10% on the $\sqrt{3}$ alloy.

Given the similarity of the bond strength of H(D) on Pt(1 1 1) and the (2×2) surface alloy, we conclude that structure sensitivity accounts for the majority of the observed increase in σ^R between the three surfaces. Similar effects have been observed by Zecho et al. [69] in comparing H(D) abstraction reactions from different low-index faces of Pt. However, σ^R on the $\sqrt{3}$ alloy would seem to have an additional contribution that results from a lower Pt–H(D) bond energy. Thus hot-atom reactions on this surface may contribute more than on the other two surfaces.

The other trend observed in Table 1 is that σ^R for the H → D reaction is slightly larger than that for D → H. Therefore, the net conclusion is that on the two Pt–Sn alloys there is only a small isotope effect (~10%) on the abstraction reaction cross-section, but that it is in the direction that $\sigma^R_{H\to D} > \sigma^R_{D\to H}$.

These results on the two alloys are compared to those of Wehner and Küppers [64,65] on Pt(1 1 1) where they obtained values of $\sigma^R_{H\to D} = 1.25$ Å^2 and $\sigma^R_{D\to H} = 1.6$ Å^2, using a hotter (1900 K) H atom source. In general, hydrogen abstraction reactions generally occur either with no isotope effect

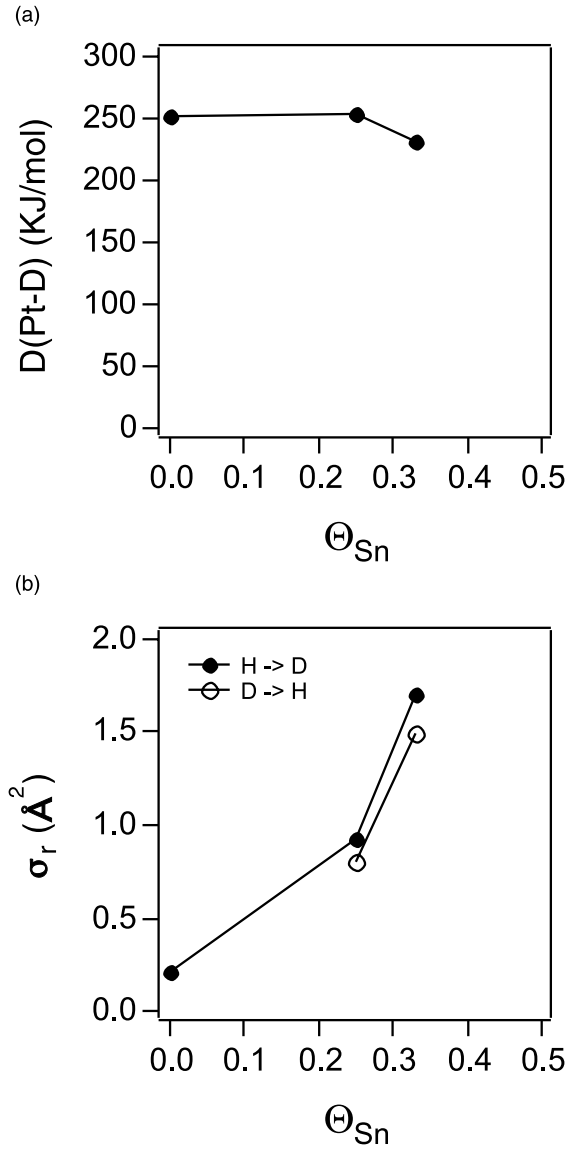

Fig. 5. (a) Pt–D bond strength on Pt(1 1 1) and the two Sn/Pt(1 1 1) surface alloys [35]. (b) Abstraction reaction cross-sections for incident H(D) with D(H) adatoms on Pt(1 1 1) and the two Sn/Pt(1 1 1) surface alloys.

or with a "normal KIE" ($\sigma^{R}_{D\to H} > \sigma^{R}_{H\to D}$) on transition metal surfaces [66]. The term "normal KIE" is derived from the fact that adsorbed H has a higher zero-point energy than adsorbed D, thus making it easier to remove by abstraction [67]. Winkler and Rendulic have outlined several physical processes during adsorption and their resulting trends in observed isotope effects [68].

However, an abstraction reaction pathway dependent on accommodation and surface migration of the incoming atom favors reaction with incoming H over D because of the mass difference. This could lead to a cancellation of the above factor (of Pt–H(D)) or perhaps even a reverse KIE ($\sigma^{R}_{H\to D} > \sigma^{R}_{D\to H}$) [68]. Our data supports this interpretation because $\sigma^{R}_{H\to D}$ for the $\sqrt{3}$ alloy is a factor of seven larger than that on Pt(1 1 1). As a final comment, reaction mechanisms involving tunneling [70] favor reaction with incoming H over D and may lead to a reverse KIE.

5. Conclusions

We report measurements of abstraction reactions of preadsorbed D(H) atoms by incident, gas-phase H(D) atoms on Pt(1 1 1) and the (2×2) and $\sqrt{3}$ Sn/Pt(1 1 1) surface alloys. While there is good understanding of such reactions on metallic surfaces, there was no data previously available on bimetallic alloys. Abstraction reactions on these Pt–Sn alloys are characterized by cross-sections σ^{R} in the 10^{-16} cm^2 range (0.8–1.7 Å^2), in the range of those values reported on other transition metal surfaces. For the H $\rightarrow$ D reaction, σ^{R} increased from 0.21 Å^2 on Pt(1 1 1) to 0.93 Å^2 on the (2×2) alloy and 1.7 Å^2 on the $\sqrt{3}$ alloy. The same trend was observed for the D $\rightarrow$ H reaction, with σ^{R} increasing from 0.8 Å^2 on the (2×2) alloy to 1.5 Å^2 on the $\sqrt{3}$ alloy. Given that the bond strength of H(D) on Pt(1 1 1) and the (2×2) surface alloy is identical, we suggest that structure sensitivity accounts for the majority of the observed differences in behavior between the three surfaces. However, a 10% reduction in the chemisorption bond energy of H(D) on the $\sqrt{3}$ alloy compared to the (2×2) alloy leads to an additional increase in σ^{R}. We observed only a small kinetic isotope effect for the abstraction reaction on these alloys, with the H-on-D reaction cross-section being slightly larger (10%) than that for D-on-H.

Acknowledgements

Financial support of this work by the Army Research Office and the Department of Energy is gratefully acknowledged. We thank Prof. Dr. Gerhard Ertl for suggesting the Pt tube source to us, and Drs. J. Wintterlin and J. Küppers for details and schematics for the design of the H-atom doser.

References

[1] E.W. Kuipers, A. Vardi, A. Danon, A. Amirav, Phys. Rev. Lett. 66 (1991) 116.
[2] C.T. Rettner, H.A. Michelsen, D.J. Auerbach, C.B. Mullins, J. Chem. Phys. 94 (1991) 7499.
[3] C.T. Rettner, Phys. Rev. Lett. 69 (1992) 383.
[4] B. Jackson, M. Persson, Surf. Sci. 269–270 (1992) 195.
[5] B. Jackson, M. Persson, J. Chem. Phys. 96 (1992) 2378.
[6] M. Xi, B.E. Bent, J. Phys. Chem. 97 (1993) 4167.
[7] D.D. Koleske, S.M. Gates, B. Jackson, J. Chem. Phys. 101 (1994) 3301.
[8] C. Lutterloh, A. Schenk, J. Biener, B. Winter, J. Küppers, Surf. Sci. 316 (1994) L1039.
[9] B.D. Thoms, J.N. Russell Jr., P.E. Pehrsson, J.E. Butler, J. Chem. Phys. 100 (1994) 8425.
[10] C.C. Cheng, S.R. Lucas, H. Gutleben, W.J. Choyke, J.T. Yates, J. Am. Chem. Soc. 114 (1992) 1249.
[11] D.D. Koleske, S.M. Gates, J. Chem. Phys. 98 (1993) 5091.
[12] B. Jackson, M. Persson, B.D. Kay, J. Chem. Phys. 100 (1994) 7687.
[13] M. Xi, B.E. Bent, J. Vac. Sci. Technol. B 10 (1992) 2440.
[14] J. Biener, U.A. Schubert, A. Schenk, B. Winter, C. Lutterloh, J. Küppers, J. Chem. Phys. 99 (1993) 3125.
[15] W.J. Mitchell, Y. Wang, J. Xie, W.H. Weinberg, J. Am. Chem. Soc. 115 (1993) 4381.
[16] J. Xie, W.J. Mitchell, K.J. Lyons, Y. Wang, W.H. Weinberg, J. Vac. Sci. Technol. A 12 (1994) 2210.
[17] J. Xie, W.J. Mitchell, K.J. Lyons, W.H. Weinberg, J. Chem. Phys. 101 (1994) 9195.
[18] K. Son, M. Mavrikakis, J.L. Gland, J. Phys. Chem. 99 (1995) 6270.
[19] B.E. Bent, Chem. Rev. 96 (1996) 1361.
[20] J. Biener, A. Schenk, B. Winter, C. Lutterloh, U.A. Schubert, J. Küppers, Surf. Sci. 307–309 (1994) 228.
[21] V. Lossev, J. Küppers, Surf. Sci. 284 (1993) 175.
[22] D.K. Zerkle, M.D. Allendorf, M. Wolf, O. Deutschmann, J. Catal. 196 (2000) 18.
[23] M.C. Huff, L.D. Schmidt, AIChE J. 42 (1996) 3484.
[24] M. Huff, L.D. Schmidt, J. Phys. Chem. 97 (1993) 11815.
[25] D.W. Flick, M.C. Huff, Catal. Lett. 47 (1997) 91.
[26] K. Baberschke, M. Farle, M. Zomack, Appl. Phys. A 44 (1987) 13.
[27] A.S. Bodke, D.A. Olschki, L.D. Schmidt, E. Ranzi, Science 285 (1999) 712.
[28] G. Eilmsteiner, W. Walkner, A. Winkler, Surf. Sci. 352–354 (1996) 263.
[29] U. Bischler, P. Sandl, E. Bertel, T. Brunner, W. Brenig, Phys. Rev. Lett. 70 (1993) 3603.
[30] A.D. Johnson, K.J. Maynard, S.P. Daley, Q.Y. Yang, S.T. Ceyer, Phys. Rev. Lett. 67 (1991) 927.
[31] T. Kammler, S. Wehner, J. Küppers, Surf. Sci. 339 (1995) 125.
[32] S.H. Overbury, D.R. Mullins, M.T. Paffett, B.E. Koel, Surf. Sci. 254 (1991) 45.
[33] A. Atrei, U. Bardi, G. Rovida, M. Torrini, E. Zanazzi, P.N. Ross, Phys. Rev. B 46 (1992) 1649.
[34] M. Galeotti, A. Atrei, U. Bardi, G. Rovida, M. Torrini, Surf. Sci. 313 (1994) 349.
[35] M.R. Voss, H. Busse, B.E. Koel, Surf. Sci. 414 (1998) 330.
[36] M.T. Paffett, S.C. Gebhard, R.G. Windham, B.E. Koel, J. Phys. Chem. 94 (1990) 6831.
[37] P. Samson, A. Nesbitt, B.E. Koel, A. Hodgson, J. Chem. Phys. 109 (1998) 3255.
[38] E.K. Rideal, Proc. Cam. Phil. Soc. 35 (1938) 130.
[39] D.D. Eley, E.K. Rideal, Nature 146 (1940) 401.
[40] I. Langmuir, Trans. Faraday Soc. 17 (1922) 621.
[41] C.N. Hinshelwood, E.J. Bowen, Phil. Mag. 40 (1920) 569.
[42] T.A. Jachimowski, W.H. Weinberg, J. Chem. Phys. 101 (1994) 10997.
[43] W.H. Weinberg, Acc. Chem. Res. 29 (1996) 479.
[44] A. Sellidj, B.E. Koel, J. Phys. Chem. 97 (1993) 10076.
[45] B. Poelsema, L.K. Verheij, G. Comsa, Surf. Sci. 152/153 (1985) 496.
[46] M.T. Paffett, R.G. Windham, Surf. Sci. 208 (1989) 34.
[47] P.R. Norton, J.A. Davies, T.E. Jackman, Surf. Sci. 121 (1982) 103.
[48] K. Christmann, G. Ertl, T. Pignet, Surf. Sci. 54 (1976) 365.
[49] T. Engel, K.-H. Rieder, in: D.A. King, D.P. Woodruff (Eds.), The Chemical Physics of Solid Surfaces and Heterogeneous Catalysis, vol. 4, Elsevier, Amsterdam, 1982, p. 125.
[50] R.C. Weast (Ed.), CRC Handbook of Chemistry and Physics, vol. 70, CRC Press, Boca Raton, FL, 1989.
[51] K. Christmann, Surf. Sci. Rep. 9 (1988) 1.
[52] R.E. Honig, D.A. Kramer, RCA Rev. 30 (1969) 285.
[53] A. Winkler, J. Vac. Sci. Technol. A 5 (1987) 2430.
[54] K. Jousten, P. Röhl, Vacuum 46 (1995) 9.
[55] A.V. Teplyakov, B.E. Bent, J. Chem. Soc. Faraday Trans. 91 (1995) 3645.
[56] S.T. Ceyer, Science 249 (1990) 133.
[57] J. Harris, B. Kasemo, Surf. Sci. 105 (1981) L281.
[58] C.T. Rettner, D.J. Auerbach, Science 263 (1994) 365.
[59] C.T. Rettner, D.J. Auerbach, Surf. Sci. 357/358 (1996) 602.
[60] C.T. Rettner, Phys. Rev. Lett. 69 (1992) 383.
[61] C.T. Rettner, D.J. Auerbach, Phys. Rev. Lett. 74 (1995) 4551.
[62] C.T. Rettner, D.J. Auerbach, J. Chem. Phys. 104 (1996) 2732.
[63] P. Kisliuk, J. Phys. Chem. Solids 3 (1957) 95.

[64] S. Wehner, J. Küppers, J. Chem. Phys. 108 (1998) 3353.
[65] S. Wehner, J. Küppers, Surf. Sci. 411 (1998) 46.
[66] M.J. Weiss, C.J. Hagedorn, W.H. Weinberg, Surf. Sci. 429 (1999) 54.
[67] R.P. Bell, The Tunnel Effect in Chemistry, Chapman & Hall, New York, 1980.
[68] A. Winkler, K.D. Rendulic, Int. Rev. Phys. Chem. 11 (1992) 101.
[69] Th. Zecho, B. Brandner, J. Küppers, Surf. Sci. 418 (1998) L26.
[70] R. Baer, Y. Zeiri, R. Kosloff, Surf. Sci. 411 (1998) L783.